Aleksandr M. Golubev, Eva Brücher, Armin Schulz, Reinhard K. Kremer* and Robert Glaum

La- and Lu-agardite – preparation, crystal structure, vibrational and magnetic properties

https://doi.org/10.1515/znb-2019-0189
Received November 8, 2019; accepted November 21, 2019

Abstract: Polycrystalline samples of La- and Lu-agardite with the composition $RECu_6(OH)_6(AsO_4)_3 \cdot n\ H_2O$ (RE = La, Lu; $n \approx 3$) have been prepared and the structure of the products was determined by X-ray powder diffraction studies. The characterization has been complemented by Raman and UV/Vis spectroscopic, magnetic and TGA investigations. DFT calculations support the conclusions drawn from the experiments. The arsenates $RECu_6(OH)_6(AsO_4)_3 \cdot n\ H_2O$ (RE = La, Lu; $n \approx 3$) are isostructural with the mineral mixite and crystallize with a hexagonal structure which contains ribbons of edge-sharing $[CuO_5]$ square-pyramids extending along the hexagonal axis. They are interconnected via $(AsO_4)^{3-}$ groups to form hexagonal tubes of about 10 Å inner diameter. Such zeolite-like tubes host water molecules, which can be reversibly removed at moderate temperatures ($T \approx 100$°C). Like in mixite and $YCu_6(OH)_6(AsO_4)_3 \cdot 3\ H_2O$, the Cu^{2+} cations in $RECu_6(OH)_6(AsO_4)_3 \cdot n\ H_2O$ (RE = La, Lu; $n \approx 3$) exhibit low-dimensional antiferromagnetic properties, which are subject to changes in the Cu–O–Cu bond lengths and angles due to the lanthanide contraction.

Keywords: agardite; crystal structure; DFT calculations; low-dimensional quantum antiferromagnet; magnetic properties; mixite; vibrational spectroscopy.

Dedicated to: Professor Dr. rer. nat. Dr. h.c. mult. Arndt Simon on the occasion of his 80th birthday.

1 Introduction

Stimulated by the discovery of high-T_c superconductivity in oxocuprates, low-dimensional quantum antiferromagnets have attracted particular attention in the last three decades [1]. Despite extensive research, the coupling mechanism of high-T_c superconductors is still disputed. Especially, it is still controversial how and to what extent magnetic excitations of the two-dimensional cuprate layers play a role for high-T_c superconductors [2, 3]. Another interesting aspect of low-dimensional quantum magnets, possibly intimately connected to the problem of high-T_c superconductivity, is that instead of attaining a long-range ordered magnetic ground state the systems may condense into a spin liquid, i.e. a state where spin disorder is preserved still at lowest temperatures [4]. Numerous low-dimensional magnetic systems have been experimentally examined in the search for spin-liquid characteristics. Recently, several Cu^{2+} containing natural minerals like azurite, malachite, green and black dioptase, to name a few, came into the focus of the research for spin liquids [5]. The immediate advantage of natural minerals is that very often large and well-grown crystals are cheaply available. However, natural minerals quite often contain the magnetic entities in several different crystallographic environments hampering an unambiguous characterization, e.g. of the magnetic and thermal bulk properties. In addition, such minerals contain crystal water molecules or also hydroxyl groups with hydrogen bonds leaving an assignment of the relevant spin exchange pathways sometimes highly burdensome [6–8]. Over the last decade, density functional (DFT) calculations of spin exchange paths have made significant progress allowing a better understanding of the spin structure [9]. However, DFT calculations often rely on crystal structure data, which frequently remain only tentative, particularly at low temperatures and with respect to positions of the lighter atoms like O or H.

Recently, we have reported on the investigation of the structural, magnetic, and vibrational properties of the Cu^{2+} mineral mixite, $(Bi,Ca)Cu_6(OH)_6(AsO_4)_3 \cdot 3\ H_2O$, which we compared with artificially prepared mixite and $YCu_6(OH)_6(AsO_4)_3 \cdot 3\ H_2O$, where trivalent Bi^{3+} is replaced by Y^{3+} [10]. Mixite and $YCu_6(OH)_6(AsO_4)_3 \cdot 3\ H_2O$ crystallize in the space group $P6_3/m$ (no. 176) with a 'zeolite-type' structure (Fig. 1). Tri-capped trigonal prisms $[REO_9]$ (with six oxygen atoms from arsenate anions and three hydroxide groups; see Figs. 1 and 4) and square-pyramidal $[CuO_5]$ groups (three oxygen atoms from arsenate anions and two hydroxide groups; see Figs. 1 and 6) together with the arsenate groups form a honeycomb arrangement of tubes of about 10 Å inner diameter propagating along

***Corresponding author: Reinhard K. Kremer,** Max-Planck-Institut für Festkörperforschung, Heisenbergstraße 1, 70569 Stuttgart, Germany, e-mail: rekre@fkf.mpg.de
Aleksandr M. Golubev, Eva Brücher and Armin Schulz: Max-Planck-Institut für Festkörperforschung, Heisenbergstraße 1, 70569 Stuttgart, Germany
Robert Glaum: Institut für Anorganische Chemie, Universität Bonn, Gerhard-Domagk-Straße 1, D-53121 Bonn, Germany

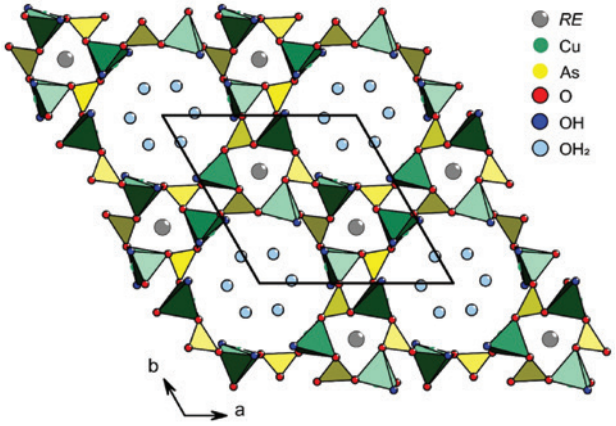

Fig. 1: Crystal structure of the compounds $RECu_6(OH)_6(AsO_4)_3 \cdot n\ H_2O$ (RE = La, Y, Lu; $n \approx 3$). Cu, As, and RE atoms are depicted by green, yellow, and grey spheres, respectively. Oxygen atoms of arsenate, hydroxide, and water are distinguished (see color code). Hydrogen atoms are not shown. A unit cell is outlined.

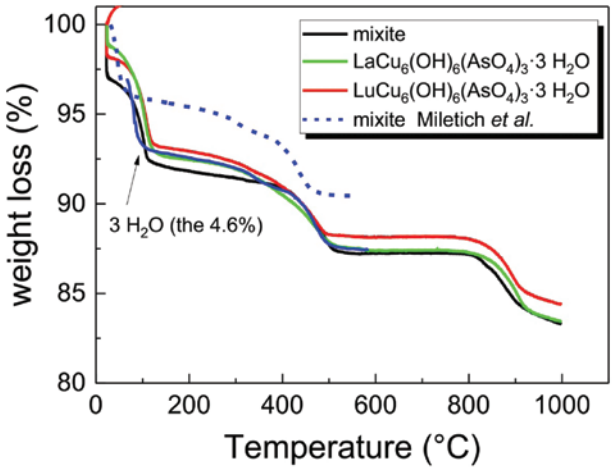

Fig. 2: (solid lines) TGA traces of synthetic mixite $BiCu_6(OH)_6(AsO_4)_3 \cdot n\ H_2O$ ($n \approx 3$), (preparation see ref. [10], La-and Lu-agardite ($RECu_6(OH)_6(AsO_4)_3 \cdot n\ H_2O$ (RE = La, Lu; $n \approx 3$) (green and red, respectively) compared to a TGA trace collected by Miletich et al. [13] on synthetic mixite (blue). The latter trace has been downshifted by 3%, and the temperature scale has been upshifted by 35°C. The blue dotted curve represents Miletich's original data.

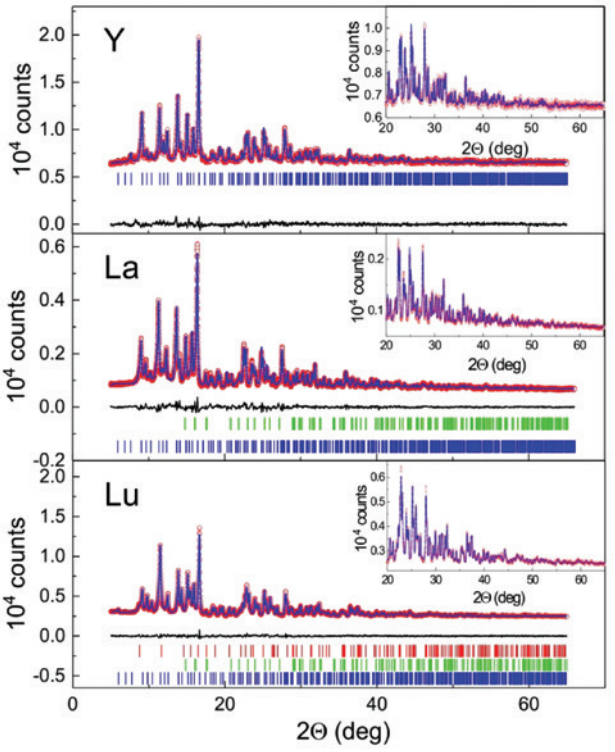

Fig. 3: X-ray diffraction patterns of $RECu_6(OH)_6(AsO_4)_3 \cdot n\ H_2O$ (RE = La, Y, Lu; $n \approx 3$), from top to bottom. The red dots mark the measured counts, the (blue) solid lines the results of the Rietveld refinement. The (black) solid lines underneath represent the differences between measured and calculated patterns. The vertical bars mark the Bragg angles of the reflections used to simulate the pattern. The (blue) bars relate to the phases $RECu_6(OH)_6(AsO_4)_3 \cdot n\ H_2O$ (RE = La, Y, Lu; $n \approx 3$); the green and red vertical bars mark the Bragg positions of CuO and $LuAsO_4$ impurity phases, respectively (for more details see text). The insets display the high-angle regions in an enlarged scale.

the hexagonal axis [11–14]. These tubes are containing up to three, highly disordered water molecules, apparently without immediate coordination to the Cu^{2+} ions. The water molecules can easily be removed in a diffusion controlled process by heating the compounds to moderate temperatures ($T \approx 100$°C). However, this dehydration is reversible [13]. As members of the mixite group, agardites in which the trivalent cation position is substituted by Al, form a series of natural minerals [15]. Natural agardite specimens generally represent solid solutions either at the trivalent metal atom site or through a replacement of As atoms by P atoms. Frost et al. [16] have synthesized and investigated the series $RECu_6(OH)_6(AsO_4)_3 \cdot 3\ H_2O$ (RE = La, Ce, Pr, Sm, Eu) by IR spectroscopy and determined the lattice parameters by X-ray powder diffraction. They reported a firm linear correlation of the lattice parameter a on the ionic radii of the RE elements with a variation from Y to La of about 1.1%. The dependence of the c lattice parameters on the ionic radii was less clearly pronounced.

In our previous publication, we have focused on the magnetic properties of natural and synthetic mixite and of $YCu_6(OH)_6(AsO_4)_3 \cdot 3\ H_2O$ with respect to possible low-dimensional magnetic behavior of the Cu^{2+} species [10]. It turned out that the magnetic properties of mixite and $YCu_6(OH)_6(AsO_4)_3 \cdot 3\ H_2O$ can be well described by a one-dimensional spin $S = 1/2$ Heisenberg behavior with alternating spin exchange of up to $\sim k_B \cdot 200$ K for mixite and

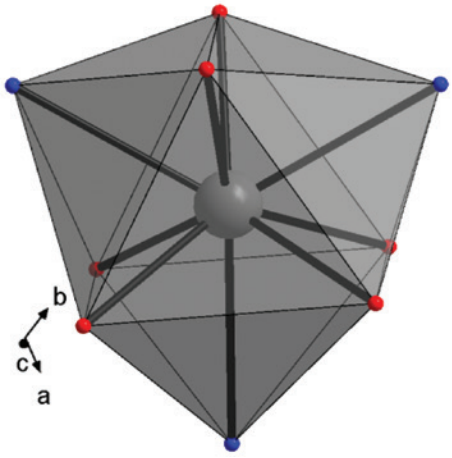

Fig. 4: Tri-capped trigonal-prismatic coordination of the *RE* atoms by oxygen atoms in $RECu_6(OH)_6(AsO_4)_3 \cdot 3\ H_2O$ (*RE* = La, Y, Lu). The red and blue spheres represent the oxygen atoms, the *RE* atom is shown by the light grey sphere. The *RE* atoms occupy the Wyckoff site 2*d* with coordinates 2/3, 1/3, 3/4.

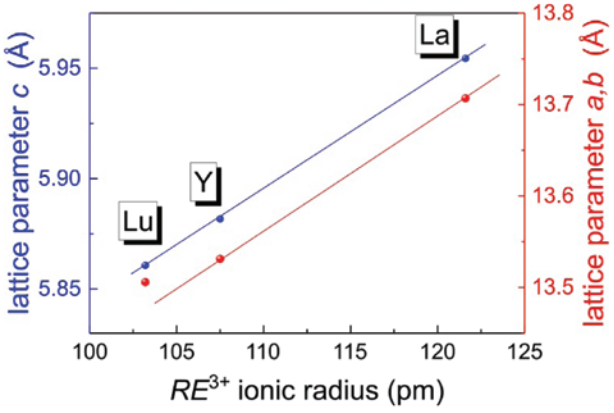

Fig. 5: Lattice parameters of $RECu_6(OH)_6(AsO_4)_3 \cdot 3\ H_2O$ (*RE* = La, Y, Lu) as a function of the ionic radii of the *RE* ions in a nine-fold coordination (ionic radii from ref. [21]).

$\sim k_B \cdot 130$ K for $YCu_6(OH)_6(AsO_4)_3 \cdot 3\ H_2O$. Long-range magnetic ordering was not found down to temperatures of 0.5 K. These experimental findings have been supported by DFT calculations. Here, we report on the continuation of this research and address the structural, vibrational, and magnetic properties of $LaCu_6(OH)_6(AsO_4)_3 \cdot 3\ H_2O$ and $LuCu_6(OH)_6(AsO_4)_3 \cdot 3\ H_2O$. La and Lu span the full *RE* series with a significant contraction of the *RE* ionic radius. The concomitant contraction of the unit cell opens the opportunity to study the magnetic behavior of an isotypic series of compounds as a function of bond lengths and angles. The significant reduction of the spin exchange parameters by reducing the *RE* ionic radius which emerged already from the comparison of the magnetic properties of mixite and $YCu_6(OH)_6(AsO_4)_3 \cdot 3\ H_2O$ is affirmed for $RECu_6(OH)_6(AsO_4)_3 \cdot 3\ H_2O$ (*RE* = La, Lu). $RECu_6(OH)_6(AsO_4)_3 \cdot 3\ H_2O$ (*RE* = La, Lu) are both found to be isotypic to mixite. Experiments to prepare $ScCu_6(OH)_6(AsO_4)_3 \cdot 3\ H_2O$ using a comparable synthesis procedures and conditions have not been not successful.

2 Experimental

Polycrystalline powders of $RECu_6(OH)_6(AsO_4)_3 \cdot n\ H_2O$ (*RE* = La, Y, Lu; $n \approx 3$) were prepared following protocols described in the literature [13, 17]. Stoichiometric mixtures of $RE(NO_3)_3 \cdot m\ H_2O$ ($3.5 < m < 6$), $Cu(NO_3)_2 \cdot 2.5\ H_2O$ and $Na_2HAsO_4 \cdot 7\ H_2O$ were dissolved in demineralized water and the products precipitated with dilute NaOH solution ($c = 1$ M). The precipitates were repeatedly washed with demineralized water and dried. X-ray diffraction patterns collected on such powders revealed a diffuse broad background but no coherent Bragg reflections. In order to

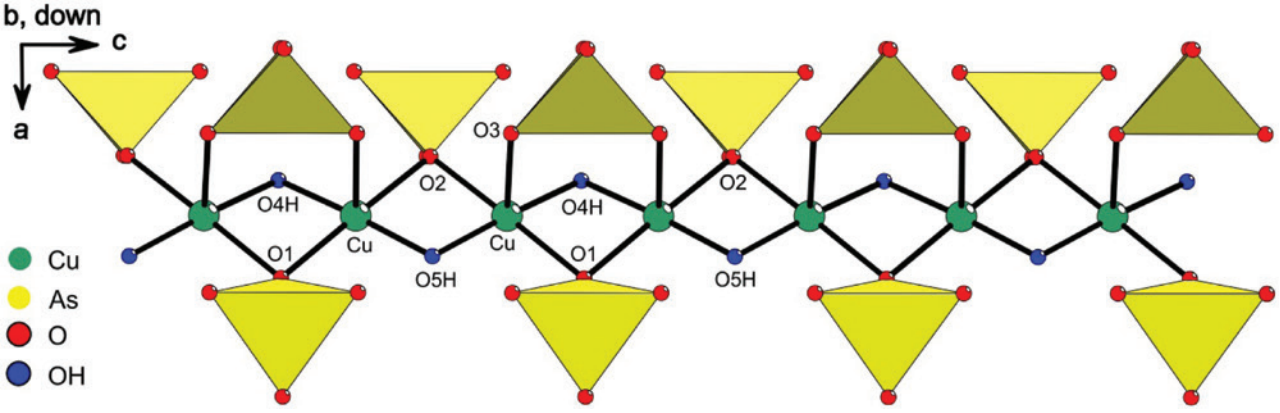

Fig. 6: Chain of edge-sharing CuO_5 square-pyramids with the $(AsO_4)^{3-}$ groups attached to oxygen atoms O1, O2, and O3, as indicated. Due to the 6_3 screw symmetry operation, the As atoms (Wyckoff site 6*h*, $z_{As} = 1/4$) are connected only to every second oxygen atom along the chains. Cu, As, O, and O (of OH) atoms are depicted by green, yellow, red and blue spheres.

improve their crystallinity, the precipitates were stirred into 10 mL demineralized water, and the slurry filled into a Teflon-lined stainless steel autoclave and heated to 175°C for 2 days. Adjusting the pH to ~8.5 before the autoclave treatment gave the best results and only small amounts of impurity phases were formed.

Non-isothermal dehydration of the samples was carried out in a Netzsch STA 449 F5-Jupiter TG setup with heating rates of 2 K min^{-1} in a flowing 20 mL min^{-1} Ar atmosphere.

Powder X-ray diffraction patterns were collected at room temperature with a Stadi-P powder diffractometer (Fa. STOE & Cie GmbH, Darmstadt, Germany), using Mo$K\alpha_1$ radiation ($\lambda = 0.7093187$ Å). The samples were sealed in 0.3 mm outer diameter quartz glass capillaries and the patterns were collected in the range $5 \le 2\theta \le 65°$. The diffraction patterns were refined using the FullProf software package using a Voigt profile function (NPR = 7) [18]. All positional and displacement parameters were refined with the constraint that displacement parameters of alike elements were assumed to be identical. The oxygen positional parameters were consistent with those given by Mereiter and Preisinger [12]. The Raman spectra were measured at room temperature with a Jobin Yvon Type V 010 LabRAM single grating spectrometer (spectral resolution ~1 cm^{-1}) using linearly polarized laser light of 532 nm wavelength. The power of the laser was typically less than 1 mW in order to avoid decomposition of the sample at the laser spot. The laser beam was focused to a 10 µm spot on the top surface of the sample using a microscope. Optical reflectance spectra were recorded at room temperature from 200 nm to 3000 nm of a polycrystalline sample diluted with $BaSO_4$ in a mass ratio 1:1 covering the NIR and the UV/Vis range using a modified CARY17 spectrophotometer. The spectrometer is equipped with an integrating sphere and was operated in the single-beam mode using $BaSO_4$ as a white reflectance standard. Magnetic properties were studied with a SQUID Magnetometer (MPMS7XL, Quantum Design, San Diego, CA, USA).

Table 1: Lattice parameters and cell volumes of $RECu_6(OH)_6(AsO_4)_3 \cdot 3\ H_2O$ (RE = La, Y, Lu).

RE	*a* (Å)	*c* (Å)	V_{cell} (Å³)
La	13.7069(1)	5.9545(1)	968.853(15)
Y	13.5313(2)	5.8818(1)	932.65(2)
Lu	13.5058(2)	5.8608(1)	925.82(3)

3 Results and discussion

3.1 Thermogravimetric investigation

Figure 2 displays the results of the thermogravimetric (TGA) measurements collected on artificial samples of mixite and on $RECu_6(OH)_6(AsO_4)_3 \cdot n\ H_2O$ (RE = La, Lu; $n \approx 3$) in comparison with a TG trace reported by Miletich et al. for artificial mixite [13]. The weight loss induced by raising the temperature revealed four distinct steps, an initial weight decrease (~3%) at about 26°C, a second ridge at about 93°C, a third and somewhat broader step between 390 and 510°C and a final weight decrease above 800°C (~3%). The very first step close to room temperature was not seen in Miletich's measurements, and we ascribe it to some residual moist in our samples. The second and third step at 90 ± 30 and 450 ± 60°C are characterized by weight losses between 4.5 and 3%, respectively, and have also been observed by Miletich et al. [13] and assigned to the complete depletion of the water molecules ('zeolitic' water, expected 4.6% for $n \approx 3$) and to irreversible thermal decomposition of the samples, probably with the loss of H_2O from the OH^- ions. The fourth step centered at about 870°C may be assigned to evaporation of decomposition products.

3.2 Powder X-ray diffraction

Figure 3 summarizes the X-ray diffraction patterns of $RECu_6(OH)_6(AsO_4)_3 \cdot 3\ H_2O$ (RE = La, Y, Lu) together with results of Rietveld refinements starting from the atom

Table 2: Refined atom positions of the atoms Cu and As in $RECu_6(OH)_6(AsO_4)_3 \cdot 3\ H_2O$ (RE = La, Y, Lu).

RE	x_{Cu}	y_{Cu}	z_{Cu}	x_{As}	y_{As}	z_{As}
La	0.41109(12)	0.09920(12)	0.5005(3)	0.6540(2)	0.14602(19)	1/4
Y	0.4102(2)	0.09434(18)	0.4993(6)	0.6529(3)	0.1519(3)	1/4
Lu	0.41164(17)	0.09685(17)	0.5022(4)	0.6558(3)	0.1531(2)	1/4

Cu and As occupy the Wyckoff position 6*h* in the space group $P6_3/m$ (no. 176). The *RE* atoms are at special Wyckoff position 2*d* (2/3, 1/3, 3/4).

positional parameters listed by Mereiter and Preisinger [12]. For $YCu_6(OH)_6(AsO_4)_3 \cdot 3\,H_2O$ the Rietveld refinement assured phase purity, whereas for $RECu_6(OH)_6(AsO_4)_3 \cdot 3\,H_2O$ (*RE* = La, Lu) small impurity Bragg reflections were detected. These could be attributed to CuO (space group *C*2/*c*; ref. [19] (5.1% weight fraction)) for *RE* = La and CuO (1.9% weight fraction) together with $LuAsO_4$ ($ZrSiO_4$ structure type; ref. [20] (11.5% weight fraction)) for *RE* = Lu.

Tables 1 and 2 compile the lattice parameters and the positional parameters of the Cu and As atoms, at Wyckoff position 12*i* and 6*h*, respectively. The *RE* atoms reside in a tri-capped trigonal prism with a 6 + 3 oxygen coordination (see Fig. 4) at Wyckoff position 2*d* with coordinates 2/3, 1/3, 3/4. The lattice parameters and the cell volumes exhibit a continuous decrease from La via Y to Lu, following the decrease of the ionic radii of the *RE* ions. Whereas for the *a* lattice parameter a clear linear dependence on the ionic radius [21] is observed, *c* deviates noticeably from a linear dependence for small ionic radii, i.e. for $LuCu_6(OH)_6(AsO_4)_3 \cdot 3\,H_2O$ (see Fig. 5).

Since for the sign and magnitude of the spin exchange in and between the chains of edge-sharing square-pyramids [CuO_5] not only the interatomic distances but also the angles ∠(Cu, O, Cu) (definition see Fig. 6) are relevant, these are compiled in Fig. 7 as a function of the *RE* ionic radii.

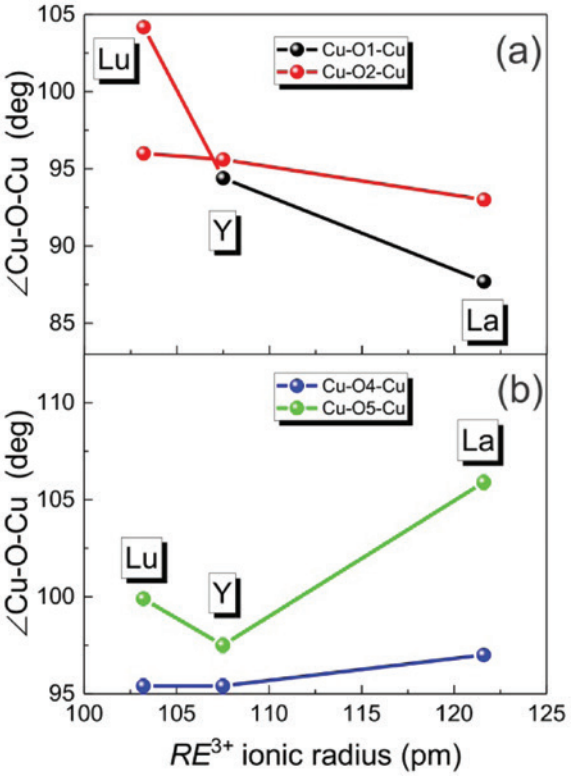

Fig. 7: Angles ∠(Cu, O, Cu) as a function of the ionic radii of the RE^{3+} cations in a nine-fold coordination. O1 and O2 atoms connect to $(AsO_4)^{3-}$, O4 and O5 atoms to OH^-. The oxygen atom labels are defined in Fig. 6.

3.3 Raman scattering

Frost et al. [16, 17, 22, 23] have extensively used Raman spectroscopy to characterize mixite samples from various mineralogical origins and proposed a first assignment of the various characteristic bands (see also the discussion in ref. [10]). One focus of this discussion was to identify the possible formation of protonated $(HAsO_4)^{2-}$ and $(H_2AsO_4)^-$ arsenate anions whose stretching vibrations can be identified by broad sideband at the high energy shoulder of the $(AsO_4)^{3-}$ Raman bands centered between 800 and 900 cm^{-1}.

Figure 8 shows a comparison of the room temperature Raman spectra of $RECu_6(OH)_6(AsO_4)_3 \cdot 3\,H_2O$ (*RE* = La, Lu) in comparison with the spectrum for $YCu_6(OH)_6(AsO_4)_3 \cdot 3\,H_2O$ which has already been reported in ref. [10]. The inset displays the energy range where $(OH)^-$ stretching vibrations are expected. Qualitatively, the spectra for $RECu_6(OH)_6(AsO_4)_3 \cdot 3\,H_2O$ (*RE* = La, Y, Lu) are very similar indicating the same structure type in support of our X-ray structure determination. Some modes are more pronounced due to intricacies to focus the laser spot on the polycrystalline particles. Quantitatively

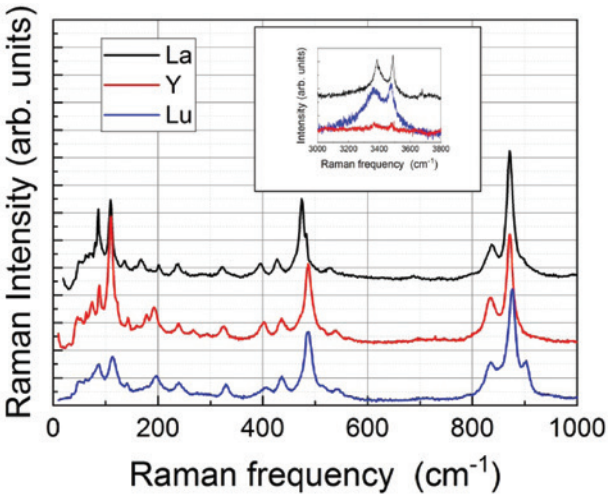

Fig. 8: Raman spectra of $RECu_6(OH)_6(AsO_4)_3 \cdot 3\,H_2O$ (*RE* = La, Y, Lu) collected at room temperature. The spectra of $RECu_6(OH)_6(AsO_4)_3 \cdot 3\,H_2O$ (*RE* = La, Y) have been up-shifted for clarity.

there are slight shifts, e.g. for the pronounced mode just below 500 cm^{-1}, which have been assigned to AsO_4 bending vibrations. From La to Lu the strongest band

is up-shifted from 474 to 488 cm^{-1}, which parallels the decreasing lattice parameters on going from La to Lu. For $LuCu_6(OH)_6(AsO_4)_3 \cdot 3\ H_2O$, it appears that the band starts to split into two overlapping modes. Similarly, the modes near 900 cm^{-1}, which have been attributed to stretching vibrations of the $(AsO_4)^{3-}$ group, exhibit an up-shift from 871 to 876 cm^{-1}, for La and Lu, respectively. Some extra splitting is discerned, e.g. of the 876 cm^{-1} mode of the $LuCu_6(OH)_6(AsO_4)_3 \cdot 3\ H_2O$ spectrum. The OH^- stretching vibrations centered at ~3500 cm^{-1} are broad but well resolved for La and Lu. The Y and Lu compounds exhibit a slight downshift of about 15–20 cm^{-1}.

3.4 UV/Vis spectroscopy and AOM

The powder reflectance spectrum of $LaCu_6(OH)_6(AsO_4)_3 \cdot 3\ H_2O$ in the NIR/UV/Vis range shows two bands at $\tilde{\nu} = 13\,700\ cm^{-1}$ (1.70 eV) and $\tilde{\nu} = 31\,900\ cm^{-1}$ (3.94 eV) and a significantly weaker band centered at approximately 5100 cm^{-1} (Fig. 9). The former clearly originates from *d*–*d* electronic transitions of the $[Cu^{II}O_5]$ chromophore. The NIR spectrum (inset Fig. 9) is very similar to that reported by Frost et al. and has been ascribed to HOH overtone vibrations [16].

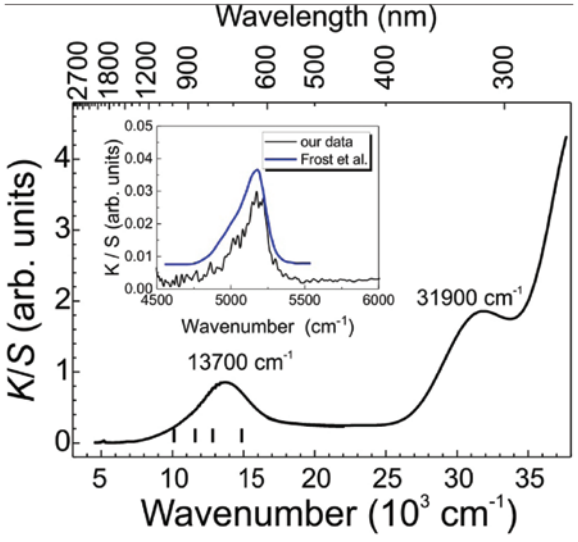

Fig. 9: Powder reflectance spectrum of $LaCu_6(OH)_6(AsO_4)_3 \cdot 3\ H_2O$. Black vertical bars mark the ligand field transition energies for the square-pyramidal $[Cu^{II}O_5]$ chromophore, obtained from AOM calculations. We show the Kubelka-Munk relation, $K/S = (1 - R_f)^2/(2R_f)$, where $R_f = I(LaCu_6(OH)_6(AsO_4)_3 \cdot 3\ H_2O)/I(BaSO_4)$. $I(LaCu_6(OH)_6(AsO_4)_3 \cdot 3\ H_2O)$ and $I(BaSO_4)$ are the reflected light intensities of the sample and the $BaSO_4$ used as white standard, respectively [24]. The inset displays the NIR spectrum given by the (black) solid line. For comparison we also show the spectrum for $LaCu_6(OH)_6(AsO4)_3 \cdot 3\ H_2O$ reported by Frost et al. (blue solid line) [16].

For the chromophore $[Cu^{II}O_5]$, strong radial and angular distortions of its ligand field are expected. For a better understanding of the correlation between the geometric distortion of the chromophore and its *d*-electron energies, calculations within the framework of the angular overlap model (AOM) [25–27] were performed. An advantage of this model is its ability to use the actual geometry of the chromophores, as determined from the crystal structure analysis. Thus, instead of using global parameters, like $10Dq$ or Δ_o, one σ and two π interactions for each ligand (in total 15 bonding parameters for a square-pyramidal chromophore) with the five 3*d* orbitals of the central cation are used for the fitting between calculated and observed transition energies. The decomposition of the global ligand field parameter ($10Dq$ or Δ_o) permits also accounting for the effects of the second coordination sphere, e.g. anisotropic π bonding of ligands [28]. In addition, mixing between the 4*s* and 3*d* orbitals of copper (*d*–*s* mixing [27, 29]) is taken into account using the *eds* parametrization in the program CAMMAG [30, 31]. To reduce the number of independent bonding parameters, constraints on the parameters were introduced. Thus, for the energy $e_\sigma(Cu^{II}–O)$, proportionality to the distance $d(Cu–O)^{-5.0}$ is assumed [32]. In general, the energy of e_π is set to one quarter of the corresponding energy e_σ in the case of an 'undisturbed' π interaction [27, 28]. In the case of the particular bonding situation encountered in $LaCu_6(OH)_6(AsO_4)_3 \cdot 3\ H_2O$, with all oxygen atoms coordinating to Cu^{2+} in the pyramidal plane showing c.n.$(O^{2-}) = 3$ (Fig. 6) a reduction of π bonding has been assumed. This is in line with the AOM parametrization for chains of edge-sharing $[M^{III}O_6]$ octahedra e.g. in phosphates MPO_4 ($CrVO_4$ structure type; M = Ti, V, Cr) [33–35]. Thus, $e_{\pi,x}$, the π interaction within the plane (Cu,O,Cu), was set to zero, while for the π interaction perpendicular to this plane $e_{\pi,y} = 1/4\ e_\sigma$ was used.

Inter-electronic repulsion is introduced into the AOM calculations via the Racah parameters *B* and *C*, and spin-orbit coupling by ξ. For the angular overlap modelling the free ion ratio $C_0/B_0 = 3.8$ (Cu^{2+}) was used and retained during the calculations [27]. Covalent contributions to the Cu–O interaction in the chromophore were considered by the nephelauxetic ratio β [$\beta = B/B_0$; $B_0(Cu^{2+}) = 1240\ cm^{-1}$] [27]. The spin-orbit coupling parameter ξ was also assumed to be reduced relative to the free ion value $\xi_0(Cu^{2+}) = 830\ cm^{-1}$ by the nephelauxetix ratio β.

For the AOM calculations a modified version of the program CAMMAG [30, 31, 36] was employed. Best fit AOM parameters for the optical spectrum of $LaCu_6(OH)_6(AsO_4)_3 \cdot 3\ H_2O$ are $B = 992\ cm^{-1}$ ($\beta = 0.80$),

$C = 3770$ cm^{-1}, $\zeta = 664$ cm^{-1}, $e_\sigma(\text{Cu–O}) \sim d(\text{Cu–O})^{-5.0}$, and $e_\sigma(\text{Cu–O})_{max} = 7200$ cm^{-1} (for O3). Using a Stevens orbital reduction parameter of $k = 0.8$ [27, 37] leads to an effective magnetic moment of $\mu = 1.87$ μ_B and to the components $g_x = 2.05$, $g_y = 2.12$, and $g_z = 2.27$ ($g_{ave} = 2.15$) of the g-tensor for the [Cu^{II}O$_5$] chromophore corresponding to a Curie constant of 0.44 cm^3 K mol^{-1}, in agreement with the experimental observation (see Table 3).

3.5 Magnetic properties

In our preceding investigations on mixite and $YCu_6(OH)_6(AsO_4)_3 \cdot 3\ H_2O$ we have found that the magnetic properties are essentially characterized by low dimensional antiferromagnetic quantum magnetism [10]. In a first approach we could model the magnetic susceptibilities of the Cu^{2+} cations ($3d^9$ electronic configuration) by the susceptibility of a spin $S = 1/2$ Heisenberg chain with alternating antiferromagnetic spin exchange along the chains summarized in the Hamiltonian [38] eq. (1).

$$\mathcal{H} = J_A \sum_i \vec{S}_{2i-1}\vec{S}_{2i} + J_B \sum_i \vec{S}_{2i}\vec{S}_{2i+1} = J_A \sum_i (\vec{S}_{2i-1}\vec{S}_{2i} + \alpha \vec{S}_{2i}\vec{S}_{2i+1}) \quad (1)$$

At first sight this model does not fully correspond to the crystal structure but gained support from DFT calculations of the spin exchange pathways. The DFT calculations identified as the dominant exchange pathways an antiferromagnetic coupling along the ribbon chains (Fig. 6) to every other neighbor. The spin exchange in a six-membered ring in the *ab* plane was found to be also antiferromagnetic but by about a factor of six smaller. The spin exchange model, according to the DFT results with the two dominant pathways, is sketched in Fig. 10. Identifying in eq. (1) J_A with J_2 and J_B with $2 \times J_4$ one expects an alternation parameter α of the order of ~0.3, consistent with the experimental findings of ~0.5 for mixite [10].

Good agreement of the magnetic susceptibility with that of an antiferromagnetic Heisenberg $S = 1/2$ chain with alternating exchange coupling is also found for $LaCu_6(OH)_6(AsO_4)_3 \cdot 3\ H_2O$ as shown in Fig. 11a. Whereas the magnetic susceptibilities of $LaCu_6(OH)_6(AsO_4)_3 \cdot 3\ H_2O$ and $YCu_6(OH)_6(AsO_4)_3 \cdot 3\ H_2O$ can be rather well fitted with the alternating chain model, the magnetic susceptibility of $LuCu_6(OH)_6(AsO_4)_3 \cdot 3\ H_2O$ shares some similarities with those of mixite, and $RECu_6(OH)_6(AsO_4)_3 \cdot 3\ H_2O$ (La, Y) but cannot be fitted to the alternating exchange Heisenberg chain model eq. (1). However, a trend that immediately becomes apparent from the experimental data is the decrease of the magnitude of the overall antiferromagnetic spin exchange on going from $LaCu_6(OH)_6(AsO_4)_3 \cdot 3\ H_2O$ to $LuCu_6(OH)_6(AsO4)_3 \cdot 3\ H_2O$. This is already signaled by the downshift of the broad short range order maximum and also by the decrease of the Curie-Weiss temperature (see Table 3) obtained from a fit of the high temperature susceptibilities ($175 \le T \le 300$ K) to the Curie-Weiss law eq. (2),

$$\chi_{mol}(T) = \frac{C}{T - \theta_{CW}} + \chi_0 \quad (2)$$

where C is the Curie constant and χ_0 is a temperature-independent contribution that takes care of the diamagnetism of the closed electron shells and of the van Vleck paramagnetism. Compared to $LaCu_6(OH)_6(AsO_4)_3 \cdot 3\ H_2O$ the temperatures of the susceptibility maximum of $YCu_6(OH)_6(AsO_4)_3 \cdot 3\ H_2O$ and $LuCu_6(OH)_6(AsO_4)_3 \cdot 3\ H_2O$ decrease by a factor of two and five, respectively. The Curie-Weiss temperatures, which are a measure of the sum of the spin exchange with the neighboring magnetic partners, drop by a factor of two.

As already observed for mixite, heat capacity measurements on $RECu_6(OH)_6(AsO_4)_3 \cdot 3\ H_2O$ (RE = La, Y) showed no indication of an anomaly characteristic for long-range magnetic order [10, 39].

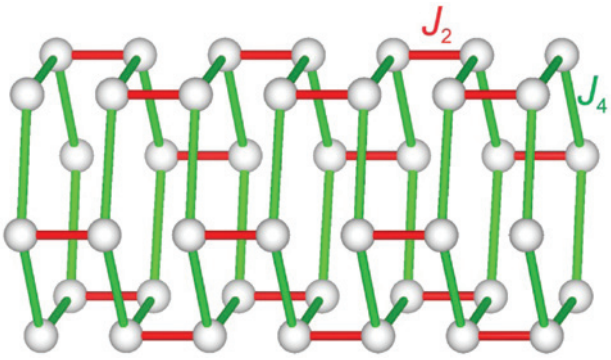

Fig. 10: Cu six-membered rings in $RECu_6(OH)_6(AsO_4)_3 \cdot 3\ H_2O$ with the dominant spin exchange parameters indicated. Spin exchange labels according to ref. [10].

Table 3: Spin exchange parameters of $RECu_6(OH)_6(AsO_4)_3 \cdot 3\ H_2O$ obtained from fits to eq. (1) and Curie-Weiss temperature θ_{CW} from fits of eq. (2) to the high-temperature susceptibilities.

RE	J_A (K)	α	θ_{CW} (K)	Ref.	C (cm^3 K per mol Cu)
La	213(3)	0.56(2)	−202(3)	This work	0.448(3)
Y	128(1)	0.76(1)	−97(1)	[10]	0.393(2)
Lu	–	–	−92(1)	This work	0.415(3)
Nat. mixite	206(2)	0.52(1)	−176(2)	[10]	0.488(5)

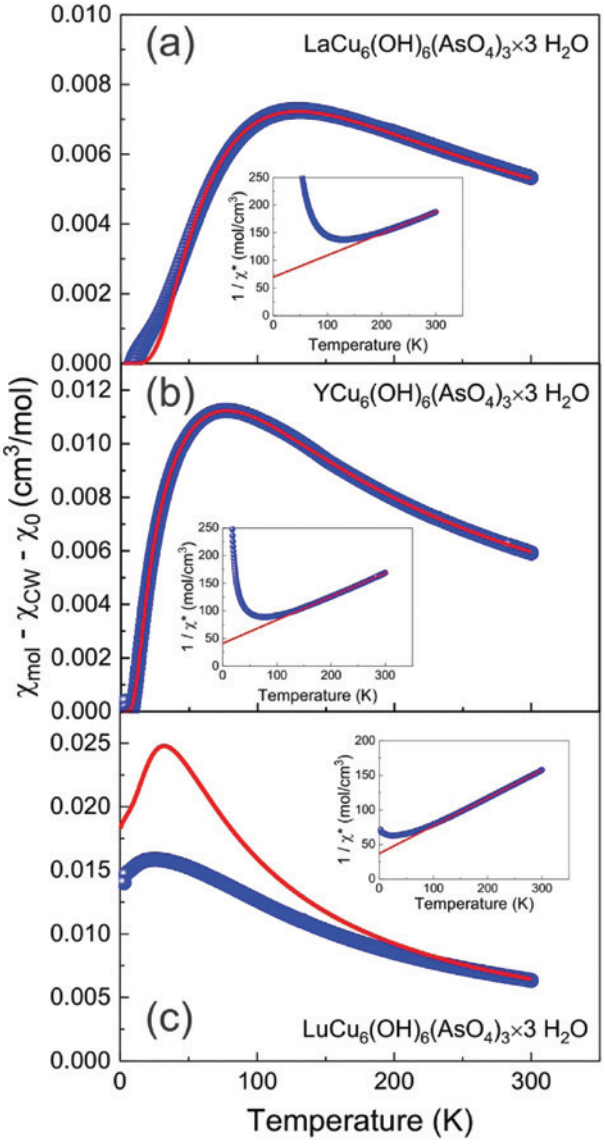

Fig. 11: Magnetic susceptibilities of compounds $RECu_6(OH)_6(AsO_4)_3 \cdot 3\ H_2O$ corrected for a temperature independent contribution and a Curie tail at low temperatures due to single-ion magnetic species. The (red) solid lines in case of La and Y represents a fit with a spin S = 1/2 Heisenberg chain with alternating antiferromagnetic spin exchange according to eq. (1) with parameters listed in Table 3. The (red) solid line in (c) represents the susceptibility of a spin S = 1/2 Heisenberg chain with uniform nearest-neighbor antiferromagnetic spin exchange of 50 K calculated according to ref. [38]. The insets display the inverse susceptibility together with a fit of the Curie-Weiss law eq. (2) to the data for $T > 175$ K. The fitted parameters are listed in Table 3.

4 Discussion and conclusion

We have prepared polycrystalline samples of two new members of the mixite/agardite mineral family with composition $RECu_6(OH)_6(AsO_4)_3 \cdot 3\ H_2O$ (*RE* = La, Lu), determined their crystal structures and investigated the desorption of crystal water, their vibrational spectra and their magnetic properties. Compounds of the type $RECu_6(OH)_6(AsO_4)_3 \cdot 3\ H_2O$ (*RE* = La, Lu) are isostructural with the minerals mixite/agardite. The lattice parameters follow the lanthanide contraction leading associated with small up-shifts of Raman modes. Most pronounced, however, is the influence of the unit cell size on the magnetic properties. Like mixite and $YCu_6(OH)_6(AsO_4)_3 \cdot 3\ H_2O$, compounds $RECu_6(OH)_6(AsO_4)_3 \cdot 3\ H_2O$ (*RE* = La, Lu) behave as low-dimensional antiferromagnetic spin $S = 1/2$ antiferromagnetic quantum magnets with no indication of long range ordering.

Despite the reduced interatomic Cu–Cu distances for $YCu_6(OH)_6(AsO_4)_3 \cdot 3\ H_2O$ and $LuCu_6(OH)_6(AsO_4)_3 \cdot 3\ H_2O$ compared to mixite and $LaCu_6(OH)_6(AsO_4)_3 \cdot 3\ H_2O$, the spin exchange decreases substantially, which we ascribe to the modified ∠(Cu, O, Cu) bonding angles. For smaller RE^{3+} ionic radii the angles decrease for the O atoms which are constituents of the $(AsO_4)^{3-}$ groups, whereas they increase for those O atoms not coordinated to an As atom. ∠(Cu, O, Cu) bond angles are decisive for the spin exchange as has been exemplarily demonstrated by Hay, Thibeault, and Hoffmann for pairs of Cu atoms bridged by an OH^- ion [40]. Especially, ∠(Cu, O, Cu) bond angles close to 90° are very critical for the magnitude and sign of the spin exchange [41] with a transition from weak ferromagnetic to antiferromagnetic spin exchange close to ~97°. From the crystal structure, the similarity of the magnetic behavior to that of an alternating chain it is not immediately evident since Cu–O–Cu spin exchange principally could take place also via the hydroxide oxygen atoms. The applicability of the alternating chain model was indicated by DFT calculations, and can be reasoned as a consequence of the different bond angles [10, 39]. A complex interplay of the angle dependence and magnetic frustration due to a competition of ferro- and antiferromagnetic exchange may be the reason why the magnetic properties of $LuCu_6(OH)_6(AsO_4)_3 \cdot 3\ H_2O$ do not correspond to those of mixite and $RECu_6(OH)_6(AsO_4)_3 \cdot 3\ H_2O$ (*RE* = La, Y). Repeated experiments to synthesize $ScCu_6(OH)_6(AsO_4)_3 \cdot 3\ H_2O$ were not successful, so far, likely due to the small ionic size of the Sc^{3+} cations.

Acknowledgements: We thank G. Siegle for measuring the heat capacities and S. Bette for collecting the TGA data.

References

[1] J. G. Bednorz, K. A. Müller, *Z. Phys. B* **1986**, *64*, 189–193.
[2] B. Keimer, S. A. Kivelson, M. R. Norman, S. Uchida, J. Zaanen, *Nature* **2015**, *518*, 179–186.

[3] A. Bussmann-Holder, A. Simon, H. Keller, A. R. Bishop, *Europhys. Lett.* **2013**, *101*, 47004-1–47004-6.
[4] L. Savary, L. Balents, *Rep. Prog. Phys.* **2017**, *80*, 016502-1–016502-55.
[5] D. S. Inosov, *Adv. Phys.* **2018**, *67*, 149–252.
[6] S. Bette, R. K. Kremer, G. Eggert, C. C. Tang, R. E. Dinnebier, *Dalton Trans.* **2017**, *46*, 14847–14858.
[7] S. Bette, R. K. Kremer, G. Eggert, R. E. Dinnebier, *Dalton Trans.* **2018**, *47*, 8209–8220.
[8] S. Bette, A. Costes, R. K. Kremer, G. Eggert, C. C. Tang, R. E. Dinnebier, *Z. Anorg. Allg. Chem.* **2019**, *645*, 988–997.
[9] H. J. Xiang, C. Lee, H.-J. Koo, X. G. Gong, M.-H. Whangbo, *Dalton Trans*. **2013**, *42*, 823–853.
[10] A. Golubev, E. Brücher, A. Schulz, R. K. Kremer, F. X. Schmidt, E. E. Gordon, M.-H. Whangbo, *Z. Anorg. Allg. Chem.* **2018**, *644*, 1782–1790.
[11] A. Schrauf, *Z. Kristallogr.* **1880**, *4*, 277–285.
[12] K. Mereiter, A. Preisinger, *Anz. Österr. Akad. Wiss. Math.-Naturwiss* **1986**, *123*, 79–81.
[13] R. Miletich, J. Zemann, M. Nowak, *Phys. Chem. Miner.* **1997**, *24*, 411–422.
[14] A. Aruga, I. Nakai, *Acta Crystallogr.* **1985**, *C41*, 161–163.
[15] T. Fehr, R. Hochleitner, *LAPIS* **1984**, *9*, 22–37.
[16] R. L. Frost, A. R. McKinnon, P. A. Williams, K. A. Erickson, M. L. Weier, P. Leverett, *N. Jb. Miner. Abh.* **2005**, *181*, 11–19.
[17] R. L. Frost, M. Weier, W. Martens, *Spectrochim. Acta A* **2006**, *63*, 685–689.
[18] J. Rodríguez-Carvajal, *Phys. B* **1993**, *192*, 55–69.
[19] S. Asbrink, L. J. Norrby, *Acta Crystallogr.* **1970**, *B26*, 8–15.
[20] G. Lohmueller, G. Schmidt, B. Deppisch, V. Gramlich, C. Scheringer, *Acta Crystallogr.* **1973**, *B29*, 141–142.
[21] The ionic radii for RE^{3+} in a nine-fold coordination have been taken from http://abulafia.mt.ic.ac.uk/shannon/ptable.php (accessed November 2019; data taken from R. D. Shannon, *Acta Crystallogr.* **1976**, *A32*, 751–767).
[22] R. L. Frost, M. Weier, W. Martens, L. Duong, *Miner. Mag.* **2005**, *69*, 169–177.
[23] R. L. Frost, J. Čejka, J. Sejkora, J. Plášil, S. Bahfenne, S. J. Palmer, *J. Raman Spectros.* **2010**, *41*, 566–570.
[24] G. Kortüm, *Reflexionsspektroskopie*, Springer-Verlag, Berlin, **1969**.
[25] C. K. Jørgensen, R. Pappalardo, H. H. Schmidtke, *J. Chem. Phys.* **1963**, *39*, 1422–1430.
[26] D. E. Richardson, *J. Chem. Educ.* **1993**, *70*, 372–380.
[27] B. N. Figgis, M. A. Hitchman, *Ligand Field Theory and its Applications*, Wiley-VCH, New York, **2000**.
[28] D. Reinen, M. Atanasov, S. L. Lee, *Coord. Chem. Rev.* **1998**, *175*, 91–158.
[29] M. J. Riley, *Inorg. Chim. Acta* **1998**, *268*, 55–62.
[30] D. A. Cruse, J. E. Davies, M. Gerloch, J. H. Harding, D. J. Mackey, R. F. McMeeking, CAMMAG, a FORTRAN program, Cambridge, **1980**.
[31] M. Gerloch, *Magnetism and Ligand-Field Analysis*, Cambridge University Press, Cambridge, **1983**.
[32] M. Bermejo, L. Pueyo, *J. Chem. Phys.* **1983**, *78*, 854–857.
[33] R. Glaum, M. A. Hitchman, *Aust. J. Chem.* **1996**, *49*, 1221–1228.
[34] R. Glaum, *Neue Untersuchungen an wasserfreien Phosphaten der Übergangsmetalle* (in German), Habilitation Thesis, University of Gießen, Gießen, **1999**. URL: http://geb.uni-giessen.de/geb/volltexte/1999/124/ (accessed November 2019).
[35] R. Glaum, H. Thauern, *Inorg. Chem.* **2007**, *46*, 2057–2066.
[36] M. Riley, CAMMAG for PC (version 4.0), University of Queensland, St.Lucia (Australia) **1997**.
[37] K. W. H. Stevens, *Proc. R. Soc. Lond. Ser. A* **1953**, *219*, 542–555.
[38] D. C. Johnston, R. K. Kremer, M. Troyer, X. Wang, A. Klümper, L Bud'ko, A. F. Panchula, P. C. Canfield, *Phys. Rev. B* **2000**, *61*, 9558–9606.
[39] A. Golubev, Dissertation, in preparation, Universität Stuttgart, Stuttgart (**2020**).
[40] P. J. Hay, J. C. Thibeault, R. Hoffmann, *J. Am. Chem. Soc.* **1975**, *97*, 4884–4899.
[41] J. B. Goodenough, *Magnetism and the Chemical Bond*, Interscience Publishers, New York, London, **1963**.